Chemistry Africa
https://doi.org/10.1007/s42250-022-00368-7

ORIGINAL ARTICLE

Biomimetic Graphene Oxide-Xanthan Gum-Hydroxyapatite Composite Scaffold for Bone Tissue Engineering

M. Vanpeene[1] · R. Rajesh[2,3] · Y. Dominic Ravichandran[3,4] · Yung-Chih Kuo[2] · Gamada Gure[4]

Received: 2 March 2022 / Accepted: 18 April 2022

Abstract

Purpose In recent years, tissue engineering scaffolds have gained popularity as a replacement for metallic/synthetic implants and tissue grafts.

Methods A porous tricomponent scaffold of graphene oxide (GO)-xanthan-hydroxyapatite (HAP) was fabricated using the freeze-drying process for bone tissue engineering.

Results The physicochemical analysis (FTIR and XRD) revealed that the composite was formed by hydrogen bonding and electrostatic interactions, and also determined a decreased crystallinity, similar to that of real bone apatite. TG/DTA analysis proved the presence of all the raw materials in the scaffold. Morphological studies supported the porous nature of HAP as well as its uniform distribution. The scaffold negatively charged functional group produced positive in vitro results in terms of cell proliferation, biocompatibility, and cell adhesion.

Conclusion The positive in vitro results confirmed that the fabricated scaffold materials could be a useful biomaterial for bone tissue engineering.

Keywords Hydroxyapatite · Graphene oxide · Xanthan gum · Scaffold · Bone tissue engineering

1 Introduction

Bones are rigid tissues that support body structure, protect internal organs, allow for movement in conjunction with muscles, and involve in the production of blood cells and the calcium storage process. [1]. As a result, a bone fracture results in serious body damage as well as excruciating pain for the patient. A variety of treatments are available when lesions unable to heal on their own. Synthetic bones are becoming more popular as a replacement for natural bone grafts [2]. Metal and ceramic implants are the most common treatment options, but with several flaws. Metal implant requires a second surgery to remove it, and shows poor tissue integration at the implantation site, resulting in infections. On the other hand, ceramics exhibit brittle nature with low tensile strength, and difficult to predict their degradation [3].

A porous three-dimensional (3D) interconnected scaffold is an attractive tissue-engineered construct because it allows cells to attach and travel within its confines (osteoconductive) while simultaneously supplying chemicals that promote progenitor cell proliferation and differentiation [4]. Biocompatible, biodegradable, and non-toxic scaffolds are necessary, and to accomplish this, develop scaffolds that duplicate human bone and have a structure similar to human bone structure. 70 % (wt.) mineral carbonated hydroxyapatite (HAP), 10% (wt.) water, and 20% (wt.) organic components make up human bone (primarily type-I collagen) [5]. Bioceramic HAP and biopolymer xanthan gum are used to mimic the natural collagen-HAP structure. Adding graphene oxide (GO) as a reinforcement material improves the mechanical characteristics of the xanthan-HAP composite even further.

✉ Y. Dominic Ravichandran
ydominic64@yahoo.co.in

1 Research and Development Department, Saint-Gobian Abrasives, Region of Paris, France

2 Department of Chemical Engineering, National Chung Cheng University, Chia-Yi, Taiwan 62102, Republic of China

3 Department of Science and Humanities, Karpagam College of Engineering, Tamil Nadu, Coimbatore 641032, India

4 Department of Chemistry, College of Natural and Computational Sciences, Wollega University, Nekemte, Ethiopia

Published online: 30 May 2022

HAP is a biocompatible ceramic substance with a structure that resembles natural bone minerals [6, 7]. HAP is also a bioactive, non-toxic, non-inflammatory, and non-immunogenic substance with osteoconductive and osteoinductive properties. HAP is extensively utilized in orthopedic implants, bone restoration, and dental implants [8]. HAP is gradually replaced by the host bone after implantation, allowing for faster bone regeneration by enhancing osteoconduction. HAP synthesis is complex, despite the fact that there are several synthetic methods for preparing HAP, such as the sol–gel approach [9] or the hydrothermal procedure [10]. In addition, the procedures are expensive, and the HAP produced is neither biocompatible, osteoconductive, or bioresorbable enough. Thermal calcination, on the other hand, is a less expensive and easier way to separate natural carbonated HAP from animal bone.

The anionic polysaccharide xanthan gum is produced by the bacteria *Xanthomonas campestris* [11]. Xanthan gum is a biocompatible polymer that can be used to transport growth components and matrices in tissue engineering [12]. It may gel in seconds in place, hold large amounts of water, and so provide an environment similar to the extracellular matrix found in nature (ECM). Furthermore, xanthan gum has antibacterial properties against *Pseudomonas aeruginosa*, *Staphylococcus aureus*, and *Staphylococcus epidermidis*, all of them responsible for bone implant failure [13].

Graphene is a planar sheet of sp^2 linked carbon atoms densely packed in a honeycomb crystal structure that is only one atom thick. It is the thinnest known material in the cosmos [14, 15]. It is also extremely robust and effective in transferring heat and electricity. As a result, in terms of mechanical and thermal properties, polymer/graphene nanocomposites surpass polymer alone. On the other hand, organic polymers are incompatible with pristine graphene. The presence of oxygen-containing groups (epoxide, hydroxyl, and carboxylic groups) on the basal plane and edges of graphene oxide (GO) sheets makes them more compatible with organic polymers, resulting in a large number of reactive sites and interactions [16, 17]. GO sheets also offer outstanding mechanical characteristics, biocompatibility, and biostability, made it an important material for tissue engineering scaffolds. On a big scale, they can be made simply and cheaply from graphite.

Nanomaterials have created tremendous impact in tissue engineering scaffolds due to their extremely smaller size, larger surface area, and potential for cells/tissue interaction. They have interesting physicochemical and biological properties for biomedical applications [18]. In this study, we analyzed the physicochemical interactions, morphology, and in vitro biological response of a new tricomponent scaffold of GO-xanthan-HAP fabricated by freeze-drying to achieve the porous nature. MTT assays confirmed that the tricomponent scaffold was biocompatible with MG 63 cells.

2 Experimental Procedure

2.1 Materials

The thermal calcinations method was used to isolate HAP from chicken bones (local slaughterhouse). Other materials were procured from various company such as, MG 63 cell line from the National Center for Cell Science, Graphite, xanthan gum, 3-(4,5-dimethylthiazol-2-yl)-2,5-diphenyltetrazolium bromide (MTT), acridine orange and bisbenzimide Hoechst 33,342 stains from Sigma Aldrich, Dulbecco's Modified Eagle's Medium (DMEM from HIMEDIA, Sodium phosphate buffer, KCl and NaCl from Merck, and NaOH, $NaNO_3$, $KMnO_4$, Con.H_2SO_4 and 30% H_2O_2 S.D. fine chemicals.

2.2 Preparation of GO

Marcano et al. [19], described the modified Hummers method for preparing GO. In 23 mL of Con. H_2SO_4, powdered flake graphite (1 g) and $NaNO_3$ (0.5 g) were mixed, cooled to 0 °C using an ice bath, and continuously stirred to maintain reaction temperature below 20 °C, followed by the slow addition of $KMnO_4$ (3 g) and removing ice bath with stirring at 35 °C for 7 h. After that, additional $KMnO_4$ (3 g) was mixed tot the reaction mixture, stirred at 35 °C for 12 h, allowed to cool to room temperature, and transferred into 400 mL of ice with 3 mL of 30% H_2O_2. Finally, the suspension was subjected to filtration and washing with 30% HCl, double-distilled (DD) water and ethanol, and dried in an oven.

2.3 Isolation of HAP from Chicken Bone

Washing the chicken bones with NaOH solution and distilled water removed the skin and flesh. After that, bones were dried at 100 °C for 5 h in an oven and crushed into small pieces in a mortar and pestle. 3 g dried chicken bones were placed in a silica crucible and calcined at 800 °C for 20 h in an electric furnace (SUNSIM, India) [5].

2.4 Preparation of GO-xanthan-HAP Scaffold

Xanthan gum (1.74 g, 29.9%) was dissolved in 100 ml of DD water by stirring at 50 °C. GO (60 mg, 0.1%) was dispersed in 30 mL of DD water for 30 min by applying sonication

before being transferred to xanthan solution and then stirred at 50 °C, for 3 h. HAP (4.2 g, 70%) was dispersed in 30 mL of DD water, slowly added to the to the reaction mixture and stirred for 24 h at 60–70 °C. Finally, 3 g/well of Go-Xanthan-HAP solution was placed in a 6-well plate and subjugated to lyophilization at − 80 °C to prepare the scaffolds.

2.5 In Vitro Biocompatibility Assay

The MTT (3-(4,5-dimethylthiazol-2-yl)-2,5-diphenyltetrazolium bromide) assay was used to ascertain the scaffold construct cell proliferation. The scaffolds, were sterilized with 75% ethanol and then with 100% ethanol. MG-63 cells (1×10^5 cells/well) were cultivated in 96-well plates for 24 h and washed twice with 100 µL of serum-free medium, followed by starvation for 1 h at 37 °C. Then, cells were injected into the sterilized scaffold material, followed by incubation at 35 °C and the medium was aspirated after the 2nd and 4th days. Finally, MTT (0.5 mg/mL) in a serum-free medium was reacted with cell cultured scaffold, incubated for 4 h at 37 °C, washed with phosphate buffer solution (PBS; 200 µL), and mixed with DMSO (100 µL). At a wavelength of 570 nm, the optical density of the purple-blue (formazan) solution was determined in a spectrophotometric microplate reader (Biorad 680). Graph pad prism6 software was applied to determine cytotoxicity.

The cell attachment and proliferation on the scaffolds were identified using Hoechst 33,342 DNA staining. In a cell culture plate, ethanol sterilized scaffold material was seeded with MG-63 cells as described above for 4 days. After that, the medium was removed and washed with PBS solution. The cells were stained for 30 min at 37 °C with 0.5 mL of Hoechst 33,342 solutions (3.5 g/mL in PBS). Finally, the stained cells were visualized and photographed using an Olympus Microscope, version 6.0, Carl Zeiss lens, Germany, after 30 min.

2.6 Characterizations

The vibrational frequency of the scaffold was examined by Fourier transformed infrared spectroscopy (FT-IR) (Jasco FTIR4100, Japan), using KBr pellet at 4000–600 cm^{-1}. X-Ray diffraction (XRD) was used to examine the phase and crystallinity of the samples (Bruker, D8 Advance X-ray Diffraction spectrophotometer, German). It was performed at room temperature with a CuKα radiation source at 1.504 Å wavelength, over an angle range of 10° to 80°, with a step size of 0.02° and a scan speed of 0.5°/min. The isolated HAP XRD value was compared to the Joint Committee on Powder Diffraction Standards (JCPDS) cards. The thermal stability of the scaffold was investigated using TGA (thermogravimetric analysis) in combination with DTA (differential thermal analysis) on an SDTQ 600 TA Instrument, USA, with a scan range of 30 to 1000 °C at 10 °C/min with continuous nitrogen flow. Field Emission Electron Microscopy (FE-SEM) was utilized to visuvalize the morphology of the scaffold and isolated HAPs (JSM- 6700F, JEOL, Japan).

3 Results and Discussion

3.1 General Observation

The tricomponent scaffold ratio is fixed by combining native bone with 70% HAP (inorganic mineral), 29% xanthan (organic substance), and 1% GO. Figure 1 shows photos of the scaffolding construction. The xanthan gum solution had a thick consistency. Due to the incorporation of dark grey graphene oxide solution, the scaffold was visualized to be grey in color. The scaffold was discovered to be porous after lyophilization.

3.2 FTIR Analysis

FTIR spectra of xanthan gum, GO, HAP, and GO-xanthan-HAP composite were recorded and compared in Fig. 2 to verify the interactions between individual components and composite formation. HAP shows the characteristic peaks of 3570, 1460, 1049, 966, 881 and 634 cm^{-1}. The characteristic bands of oxygen-containing groups revealed graphite oxidation into GO, which are –OH stretching at 3300 cm^{-1}, –COOH stretching or conjugated –C=O at 1721 cm^{-1}, C=C stretching at 1621 cm^{-1}, C–OH stretching at 1225 cm^{-1}, C–O stretching at 1051 cm^{-1}, and absorption peak of epoxy groups at 826 cm^{-1} [20]. Xanthan showed the characteristic peak of –OH stretching at 3419 cm^{-1}, C-H stretching at 2927 cm^{-1} and –C=O stretching at 1731 cm^{-1}, which correspond to the acetate and pyruvate groups, carboxylate stretching at 1641 cm^{-1}, and acetal stretching at 1136 and 1066 cm^{-1} [21, 22].

The FTIR spectra of the GO-xanthan-HAP scaffold revealed a shift in peak value as well as blended characteristic peaks from all of the constituent components. The homogeneous dispersion of GO and HAP in the xanthan gum was confirmed by the mixed characteristic peaks. The shift in peak values from 3419 to 3417 cm^{-1} and 1621 to 1610 cm^{-1} in xanthan and from 962 to 960 cm^{-1} in HAP confirmed the creation of scaffold involving ionic interaction between the constituent components. The shift in HAP peak values from 1049 to 1047 cm^{-1} also confirmed strong intermolecular hydrogen bonding between GO and HAP.

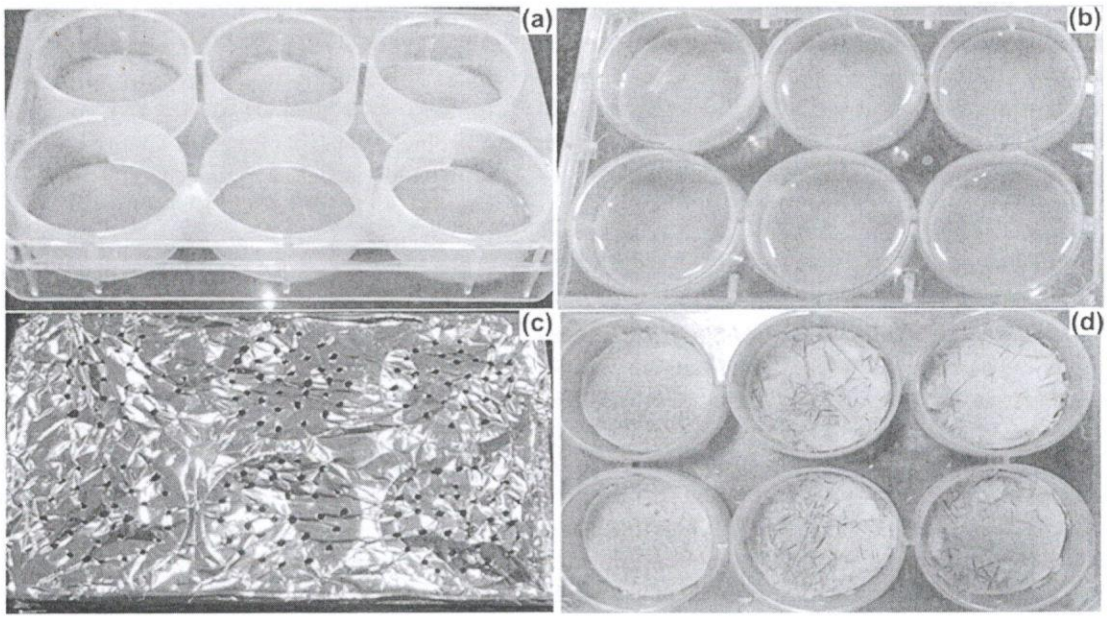

Fig. 1 Process of scaffold fabrication. **a**: empty cell culture plate (6-well). **b**: cell culture plate filled with composite solution. **c**: before lyophilization. **d**: after lyophilization

The composite scaffold formation through ionic and hydrogen bonding was corroborated by FTIR analysis [20, 23, 24].

3.3 XRD Analysis

Figure 3 shows the XRD patterns of xanthan, GO, HAP, and the GO-xanthan-HAP scaffold. The standard HAP value (JCPDS-09–0432/1996) was discovered to agree with the isolated HAP diffraction pattern. GO has a characteristic diffraction peak at a lower angle of 11.9° (*002*) and a *d*-spacing value of 0.743 nm calculated from Bragg's equation, which is within the range of values previously reported and confirms the presence of oxygen-containing groups in the interlayer spacing [25, 26]. The amorphous nature of xanthan was revealed by the broad diffraction peaks obtained at 20.3°. The intercalation of HAP in the xanthan and GO matrix with ionic interaction was confirmed by the shift in HAP peaks and the reduction in peak intensity for xanthan and GO, proving the formation of the GO-xanthan-HAP scaffold [23]. Furthermore, decreased GO and xanthan intensity confirmed decreased tricomponent scaffold crystallinity and complete GO exfoliation [14, 25]. The decreased crystallinity suggested that the GO-Xanthan-HAP scaffold crystallographic structure was more similar to natural bone mineral [27, 28].

3.4 Thermal Analysis

Figure 4 shows the TGA/DTA profile of the GO-xanthan-HAP composite. The 1.76% weight loss seen in the range of 30–150 °C is due to the elimination of integrated water molecules. In addition, the DTA curve revealed a significant endothermic peak at 277 °C, which correlated to xanthan gum disintegration and confirmed by a 13.92% weight loss from 250 to 500 °C. No substantial weight was measured at temperatures above 600 °C, indicating that all organic compounds had virtually totally disintegrated. The total weight loss was more than 25%, which is understandable given that xanthan gum accounts for 29.9% of the composite. The incinerated residue of the GO-xanthan-HAP composite mainly consisted of HAP due to its excellent stability at high temperatures [20, 29, 30]. These findings add to the evidence that all of the raw materials were present in the composite and that the scaffold was formed.

3.5 Morphology Analysis

The crystalline constitution and surface appearance of the GO-xanthan-HAP composite as evaluated by FE-SEM are shown in Fig. 5. The crystal size of HAP was determined to be 300–400 nm, and it had a flake-like crystalline structure (Fig. 4a). The scaffold has a porous structure with magnification and a homogeneous structure to the naked eye. The porous architecture of the scaffold was visible in the lower magnification image (Fig. 4b) with the integration of HAP (white crystal) in the organic matrix of xanthan gum (translucent). The higher magnification image of scaffolds (Fig. 4c) revealed a consistent distribution of HAP crystals bound to the xanthan matrix. Because GO is present in such a little amount in the composite (0.1%), and it is very highly diffused, it is not visible in the images.

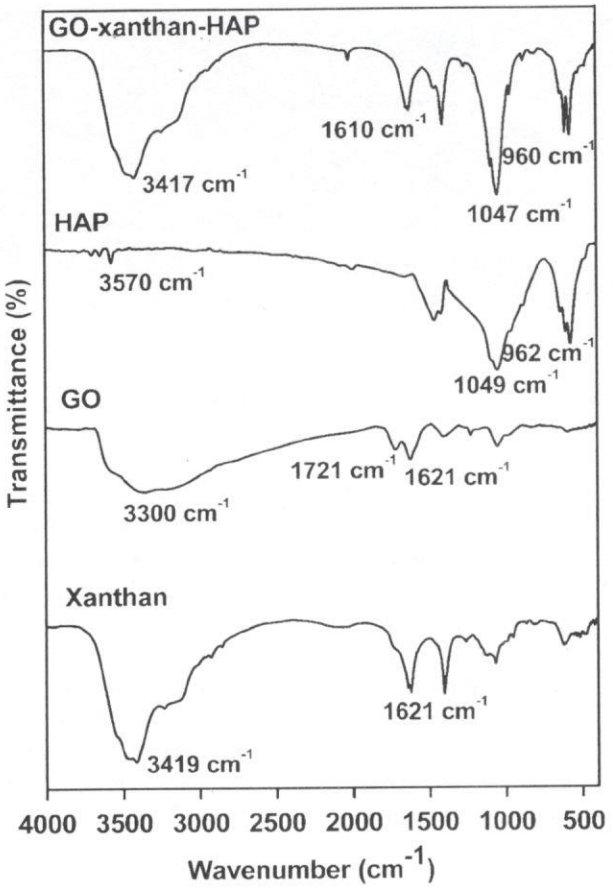

Fig. 2 FT-IR spectra of xanthan, GO, isolated HAP at 800 °C and GO-xanthan-HAP scaffold

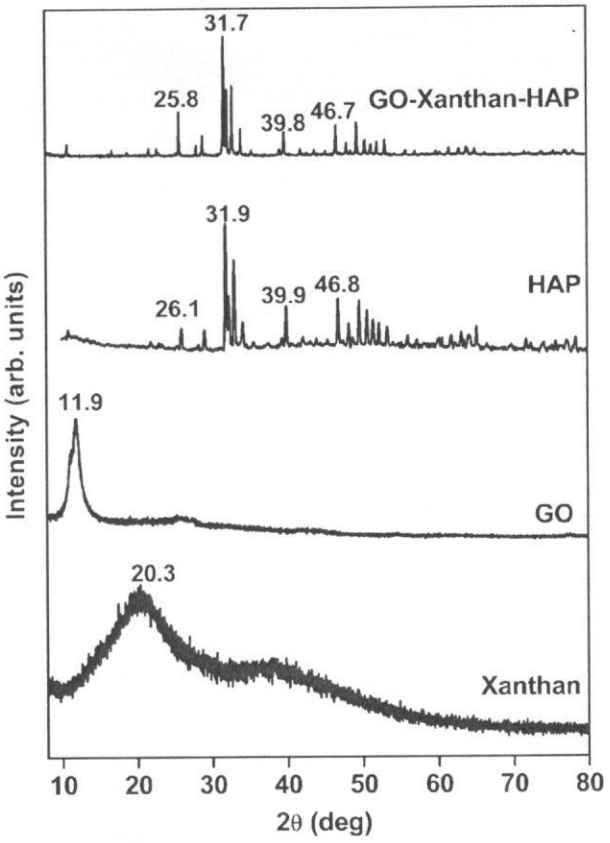

Fig. 3 XRD patterns of xanthan, GO, isolated HAP at 800 °C and GO-xanthan-HAP scaffold

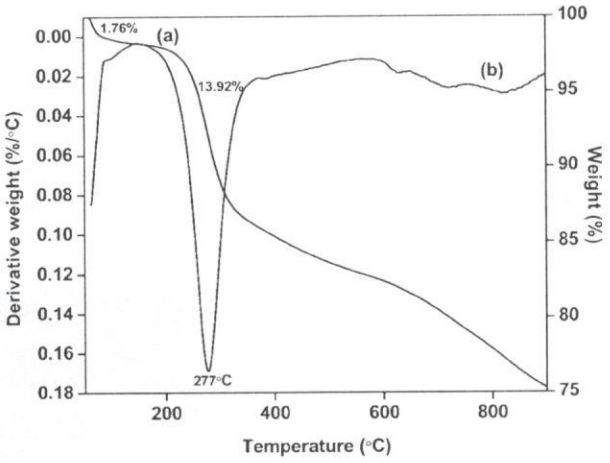

Fig. 4 DTA (**a**) and TGA (**b**) curves for GO-xanthan-HAP scaffold from 30 to 900 °C

3.6 In Vitro Biological Assay

As previously stated, since cell proliferation is favored over osteoblast activity, cell attachment and proliferation to the scaffold surface are important in biomaterial synthesis. The scaffold cytotoxicity and cell proliferation were assessed using the MTT test. Figure 6 shows the optical density (OD) of blank (medium alone) and GO-xanthan-HAP measured on the 2nd and 4th days. Because medium may offer nutrients for cell growth, it was utilized as a blank. The OD is proportional to the quantity of MTT transformed into colored formazan salt by metabolically active cells; hence, a high OD indicates a large number of living cells and indicates excellent cell proliferation on the scaffold. On day 4, the scaffold OD was much higher than the blank. As a result, the GO-xanthan-HAP composite was discovered to be biocompatible, meaning it was non-cytotoxic and allowed cell proliferation.

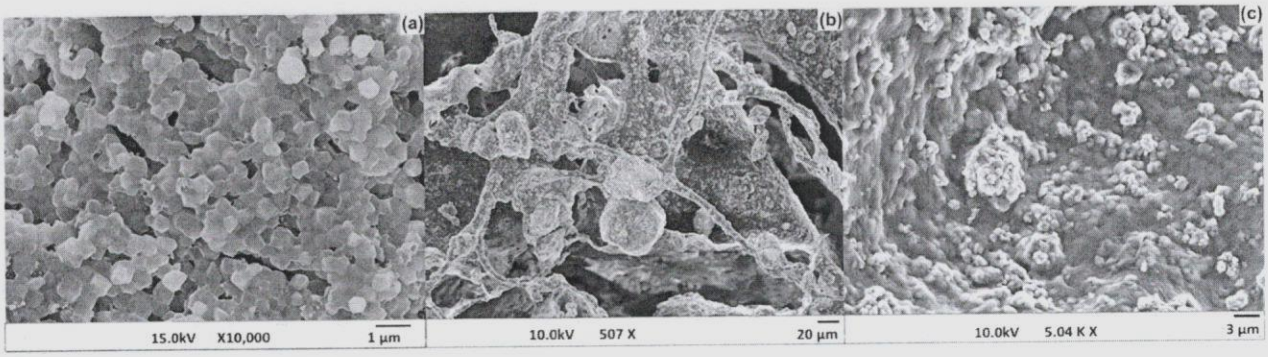

Fig. 5 FE-SEM pictures of the **a** HAP and **b**, **c** GO-xanthan-HAP scaffold. Magnification at 11 (**a**): 22.77 K X 11 (**b**): 507 X

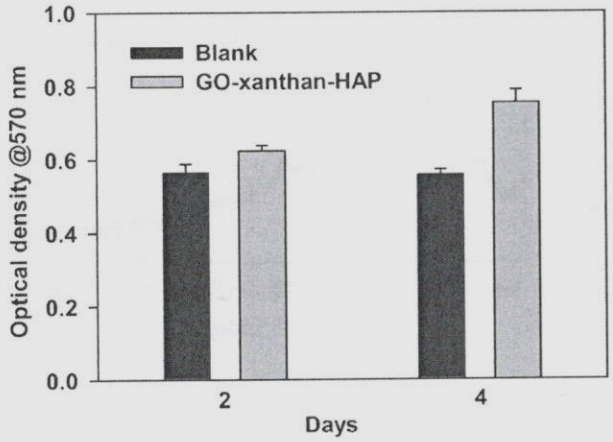

Fig. 6 Cell proliferation of MG-63 cells on GO-xanthan-HAP scaffold as a function of time, measured by MTT assay

The findings of the cell attachment assay for the GO-xanthan-HAP scaffold are shown in Fig. 7. The image depicts a high level of scaffold-osteoblast interaction and serves as an example of a useful in vitro model for researching bone cell-biomaterial interactions due to the presence of GO and xanthan gum. Because of the multiple oxygen-containing functional groups, both are polar and have a negative charge. Negative charge is a physicochemical factor that affects cell-biomaterial interactions, and negatively charged surfaces enhance osteoblast-biomaterial interactions [31]. The scaffold materials boosted cell proliferation, biocompatibility, and adhesion in the MG 63 cell line, according to in vitro investigations. As a result, GO-xanthan-HAP will be more effective in bone tissue engineering.

4 Conclusion

The development and characterization of a new GO-xanthan-HAP scaffold, as well as the research of its osteoconductivity on MG 63 cells for use in bone tissue engineering, are demonstrated in this article. The hydrogen bonding and electrostatic interactions between the components in the scaffold were revealed by FTIR analysis. Due to amorphous xanthan and GO, XRD measurements show that porous

Fig. 7 Live cell imaging with Hoechst 33,342 stain of MG63 cells cultured on GO-xanthan-HAP scaffold

scaffold has poorer crystallinity than HAP. The porosity morphology for nutrient transport and cell growth is demonstrated by FE-SEM morphology, which clearly shows the homogeneous distribution of HAP over xanthan. In vitro MTT and Hoechst stain assays revealed improved cell adherence and increased osteoconductivity. As a result of its porosity and polar functional group, which regulates cell–matrix interactions, the produced scaffold material proved biocompatible and can be employed in biomedical applications.

Acknowledgements The authors thank the management of Wollega University and Ministry of Science and Higher Education, Ethiopia, and Ministry of Science and Technology of the Republic of China (Taiwan) for providing the required facilities to carry out this research work.

Data Availability Data can be made available by request.

Declarations

Conflict of Interest The authors have no conflict of interest to disclose.

References

1. Sivakumar PM, Yetisgin AA, Sahin SB, Demir E, Cetinel S (2022) Bone tissue engineering: anionic polysaccharides as promising scaffolds. Carbohydr Polym 283:119142
2. Qu H, Fu H, Han Z, Sun Y (2019) Biomaterials for bone tissue engineering scaffolds: a review. RSC Adv 9:26252–26262
3. Ghassemi T, Shahroodi A, Ebrahimzadeh MH, Mousavian A, Movaffagh J, Moradi A (2018) Current concepts in scaffolding for bone tissue engineering. Arch Bone Jt Surg 6:90–99
4. Koons GL, Diba M, Mikos AG (2020) Materials design for bone-tissue engineering. Nat Rev Mater 5:584–603
5. Rajesh R, Hariharasubramanian A, Ravichandran YD (2012) Chicken bone as a bioresource for the bioceramic (hydroxyapatite). Phosphorus, Sulfur, Silicon Relat Elem 187:914–925
6. Yedekci B, Tezcaner A, Alshemary AZ, Yilmaz B, Demir T, Evis Z (2021) Synthesis and sintering of B, Sr, Mg multi-doped hydroxyapatites: Structural, mechanical and biological characterization. J Mech Behav Biomed Mater 115:104230
7. Gulati K, Abdal-hay A, Ivanovski S (2022) Novel nano-engineered biomaterials for bone tissue engineering. Nanomaterials 12:333
8. Sathiyavimal S, Vasantharaj S, LewisOscar F, Selvaraj R, Brindhadevi K, Pugazhendhi A (2020) Natural organic and inorganic–hydroxyapatite biopolymer composite for biomedical applications. Prog Org Coat 147:105858
9. Jaafar A, Hecker C, Arki P, Joseph Y (2020) Sol-gel derived hydroxyapatite coatings for titanium implants: a review. Bioengineering 7:127
10. He D, Zhang X, Liu P, Liu X, Chen X, Ma F, Li W, Zhang K, Zhou H (2021) Effect of hydrothermal treatment temperature on the hydroxyapatite coatings deposited by electrochemical method. Surf Coat Technol 406:126656
11. Galliano S, Bella F, Bonomo M, Viscardi G, Gerbaldi C, Boschloo G, Barolo C (2020) Hydrogel electrolytes based on xanthan gum: Green route towards stable dye-sensitized solar cells. Nanomaterials 10:1585
12. Kumar A, Rao KM, Han SS (2018) Application of xanthan gum as polysaccharide in tissue engineering: a review. Carbohydr Polym 180:128–144
13. Bacakova L, Novotna K, Parizek M (2014) Polysaccharides as cell carriers for tissue engineering: the use of cellulose in vascular wall reconstruction. Physiol Res 63:29–47
14. Yu W, Sisi L, Haiyan Y, Jie L (2020) Progress in the functional modification of graphene/graphene oxide: a review. RSC Adv 10:15328–15345
15. Olabi AG, Abdelkareem MA, Wilberforce T, Sayed ET (2021) Application of graphene in energy storage device – a review. Renew Sust Energ Rev 135:110026
16. Prakash J, Prema D, Venkataprasanna KS, Balagangadharan SN, Venkatasubbu D (2020) Nanocomposite chitosan film containing graphene oxide/hydroxyapatite/gold for bone tissue engineering. Int j biol Macromol 154:62–71
17. Rajesh R, Ravichandran YD (2015) Development of new graphene oxide incorporated tricomponent scaffolds with polysaccharides and hydroxyapatite and study of their osteoconductivity on MG-63 cell line for bone tissue engineering. RSC Adv 5:41135–41143
18. Krystyjan M, Khachatryan G, Grabacka M, Krzan M, Witczak M, Grzyb J, Woszczak L (2021) Physicochemical, bacteriostatic, and biological properties of starch/chitosan polymer composites modified by graphene oxide, designed as new bionanomaterials. Polymers 3:2327
19. Marcano DC, Kosynkin DV, Berlin JM, Sinitskii A, Sun Z, Slesarev A, Alemany LB, Lu W, Tour JM (2010) Improved synthesis of graphene oxide. ACS Nano 4:4806–4814
20. Li M, Wang Y, Liu Q, Li Q, Cheng Y, Zheng Y, Xi T, Wei S (2013) *In situ* synthesis and biocompatibility of nano hydroxyapatite on pristine and chitosan functionalized graphene oxide. J Mater Chem B 1:475–484
21. Su L, Ji WK, Lan WZ, Dong XQ (2003) Chemical modification of xanthan gum to increase dissolution rate. Carbohydr Polym 53:497–499
22. Lii C-Y, Liaw SC, Lai VM-F, Tomasik P (2002) Xanthan gum-gelatin complexes. Eur Polym J 38:1377–1381
23. Rajesh R, Hariharasubramanian A, Senthilkumar N, Ravichnadran YD (2012) A biocompatible and load bearing composite of multiwalled carbon nanotubes chitosan and natural hydroxyapatite derived from the chicken bones wasted in the slaughterhouses. Int J Pharm Pharm Sci 4:716–720
24. Venkatesan J, Pallela R, Bhatnagar I, Kim S-K (2012) Chitosan–amylopectin/hydroxyapatite and chitosan–chondroitin sulphate/hydroxyapatite composite scaffolds for bone tissue engineering. Int J Biol Macromol 51:1033–1042
25. Zhang H-B, Zheng W-G, Yan Q, Yang Y, Wang J-W, Lu Z-H, Ji G-Y, Yu Z-Z (2010) Electrically conductive polyethylene terephthalate/graphene nanocomposites prepared by melt compounding. Polymer 51:1191–1196
26. Lonita M, Pandele MA, Lovu H (2013) Sodium alginate/graphene oxide composite films with enhanced thermal and mechanical properties. Carbohydr Polym 15:339–344
27. Chen L, Hu J, Ran J, Shen X, Tong H (2014) Preparation and evaluation of collagen-silk fbroin/hydroxyapatite nanocomposites for bone tissue engineering. Int J Biol Macromol 65:1–7
28. Slama C, Jaafar H, Karouia A, Abdellaoui M (2021) Diffraction crystallite size effects on mechanical properties of nanocrystalline $(Ti_{0.8}W_{0.2})C$. Chemistry Africa 4:809–819
29. Rajesh R, Ravichnadran YD, Raj NAN, Senthilkumar N (2014) Development of a biodegradable composite

(hydroxyapatite-chitosan-coir pith) as a packing material. Polym Plast Technol Engx 53:1105–1110
30. Zohuriaan MJ, Shokrolahi F (2004) Thermal studies on natural and modified gums. Polym Test 23:575–579
31. Depan D, Girase B, Shah JS, Misra RD (2011) Structure-process-property relationship of the polar graphene oxide-mediated cellular response and stimulated growth of osteoblasts on hybrid chitosan network structure nanocomposite scaffolds. Acta Biomater 7:3432–3445